1-1-2011

Crazy heart: kinematics of the "star pile" in Abell 545

R. Salinas
Departamento de AstronomíaUniversidad de Concepción

T. Richtler
Departamento de AstronomíaUniversidad de Concepción

M. J. West
European Southern Observatory

Aaron J. Romanowsky
San Jose State University, aaron.romanowsky@sjsu.edu

E. Llyod-Davies
University of Sussex

See next page for additional authors

Recommended Citation

R. Salinas, T. Richtler, M. J. West, Aaron J. Romanowsky, E. Llyod-Davies, and Y. Schuberth. "Crazy heart: kinematics of the "star pile" in Abell 545" *Astronomy and Astrophysics* (2011). doi:10.1051/0004-6361/201116453

A&A 528, A61 (2011)
DOI: 10.1051/0004-6361/201116453

Astronomy & Astrophysics

Crazy heart: kinematics of the "star pile" in Abell 545⋆

R. Salinas[1,2], T. Richtler[1], M. J. West[2], A. J. Romanowsky[3], E. Lloyd-Davies[4], and Y. Schuberth[5]

[1] Departamento de Astronomía, Universidad de Concepción, Concepción, Chile
e-mail: [rsalinas;tom]@astro-udec.cl
[2] European Southern Observatory, Alonso de Córdova 3107, Santiago, Chile
e-mail: mwest@eso.org
[3] UCO/Lick Observatory, University of California, Santa Cruz, CA 95064, USA
e-mail: romanow@ucolick.org
[4] Astronomy Centre, University of Sussex, Falmer, Brighton BN1 9QH, UK
e-mail: E.Lloyd-Davies@sussex.ac.uk
[5] Argelander Institut für Astronomie, Auf dem Hügel 71, 53121 Bonn, Germany
e-mail: yschuber@astro.uni-bonn.de

Received 7 January 2011 / Accepted 31 January 2011

ABSTRACT

We study the structure and internal kinematics of the "star pile" in Abell 545 – a low surface brightness structure lying in the center of the cluster. We have obtained deep long-slit spectroscopy of the star pile using VLT/FORS2 and Gemini/GMOS, which is analyzed in conjunction with deep multiband CFHT/MEGACAM imaging. As presented in a previous study the star pile has a flat luminosity profile and its color is consistent with the outer parts of elliptical galaxies. Its velocity map is irregular, with parts being seemingly associated with an embedded nucleus, and others which have significant velocity offsets to the cluster systemic velocity with no clear kinematical connection to any of the surrounding galaxies. This would make the star pile a dynamically defined stellar intra-cluster component. The complicated pattern in velocity and velocity dispersions casts doubts on the adequacy of using the whole star pile as a dynamical test for the innermost dark matter profile of the cluster. This status is fulfilled only by the nucleus and its nearest surroundings which lie at the center of the cluster velocity distribution.

Key words. galaxies: clusters: individual: Abell 545 – galaxies: kinematics and dynamics – galaxies: halos – galaxies: interactions

1. Introduction

The central regions of massive galaxy clusters are fascinating places to study. Spiral galaxies are not allowed to exist in these high-density regions (Dressler 1980; Whitmore et al. 1993). Processes such as mergers, cooling flows and tidal stripping work together to often form large, extended cD galaxies (e.g. Ostriker & Tremaine 1975; Cowie & Binney 1977; Richstone 1976). Not only the density of galaxies, i.e. baryonic dark matter, but also the density of the still mysterious dark matter is highest in the centers of massive clusters. A cluster-wide cosmological dark halo (Macciò et al. 2008) of the NFW type with a virial mass of $10^{15}\,M_{\odot}$ and a virial radius of 2 Mpc encloses in its central 10 kpc a mass of $2 \times 10^{11}\,M_{\odot}$ and in its inner 1 kpc a mass of $2 \times 10^{9}\,M_{\odot}$. These values are equal to or even higher than the baryonic mass of a normal central galaxy, so one should expect dynamical situations which are very different from those in lower density regions.

An example is Abell 545. This galaxy cluster is one of the richest and most massive clusters in the Abell catalogue. Accordingly it has a high global velocity dispersion of ~1150 km s^{-1} (Salinas et al., in prep.). The central region is populated by a dense configuration of medium-bright early-type galaxies (about 25 within projected 100 kpc) while no cD galaxy is present. Instead one finds an extended, elongated structure of low surface brightness with a major axis of about 60 kpc, dubbed the "star pile" (Struble 1988). Embedded in the star pile are at least three dwarf-like galaxies, the middle one being projected onto the geometrical center of the star pile (Fig. 1). The star pile's stellar nature and that it indeed belongs to Abell 545, has been shown by Salinas et al. (2007, hereafter S+07), who also advertised the star pile as a dynamical probe for the inner dark matter profile shape. This is interesting because there is evidence that the slopes of the central dark matter profiles in some galaxy clusters are shallower than those found in simulations (Kelson et al. 2002; Sand et al. 2004, 2008; Richtler et al. 2011).

Since the baryonic density of the star pile is low, one expects the entire inner region of Abell 545 to be dark matter dominated and the dynamics of the star pile could provide important insight into the problem of whether the inner region of the dark matter halo has a cusp or a core, testing the prediction of cuspy

⋆ Based on observations taken at the European Southern Observatory, Cerro Paranal, Chile, under programme ID 080.B-0529. Also based on observations obtained at the Gemini Observatory, which is operated by the Association of Universities for Research in Astronomy, Inc., under a cooperative agreement with the NSF on behalf of the Gemini partnership: the National Science Foundation (United States), the Sscience and Technology Facilities Council (United Kingdom), the National Research Council (Canada), CONICYT (Chile), the Australian Research Council (Australia), Ministério da Ciência e Tecnologia (Brazil) and SECYT (Argentina); and on observations obtained with MegaPrime/MegaCam, a joint project of CFHT and CEA/DAPNIA, at the Canada-France-Hawaii Telescope (CFHT) which is operated by the National Research Council (NRC) of Canada, the Institut National des Science de l'Univers of the Centre National de la Recherche Scientifique (CNRS) of France, and the University of Hawaii.

Table 1. Abell 545 MegaCam observations.

	u^*	g'	r'	i'	z'
Exp. time (s)	6×720, 1×72	5×720	5×720	5×720	6×720
FWHM (in ″)	1.27	1.18	0.95	1.0	0.68
Magnitude limit (5σ)	26.5	27.1	26.3	25.5	24.8

profiles of cosmological dark matter simulations (e.g. Navarro et al. 1996). Such a faint structure may even avoid the problems that arise due to the dynamic interactions between baryons and dark matter when a central galaxy is present (El-Zant et al. 2004; Gnedin et al. 2004; Del Popolo & Kroupa 2009). However, its usage as dynamical tracer relies on the assumption that the star pile is at rest at the cluster center and that its velocity dispersion is the result of a dynamical system in equilibrium.

Until now we had no knowledge of the kinematical situation in the core region of Abell 545. The intention of this contribution is therefore to present kinematic data for the star pile and the innermost galaxies (velocities and velocity dispersions). For Abell 545, we adopt the redshift $z = 0.1585$ (Salinas et al., in prep.), which corresponds (in a standard flat universe) to an angular distance of 565 Mpc and a scale of 2.74 kpc/″.

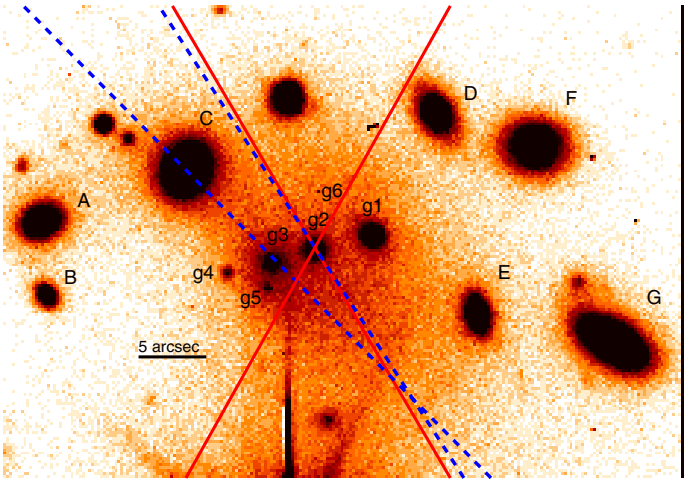

Fig. 1. A FORS1 V image excerpt showing the star pile and the longslit positioning. Red lines indicate the position of the GMOS longslits, while the blue dashed lines indicate the position of the FORS2 longslits. Faint sources, seemingly embedded in the star pile have been labeled *g1–g6*. Surrounding galaxies are labeled with letters A to G. The size of the image is $50'' \times 35''$ or 137×96 kpc at the cluster's distance. North is up and East is to the left.

2. Observations and data reduction

2.1. CFHT/MegaCam imaging

In S+07 we presented photometry of the star pile using *VRI* archival images obtained with FORS1. Here we revisit the star pile making use of deeper images retrieved from the MegaPrime/MegaCam archive (PI: G. Morrison). MegaCam is an optical camera installed at the Canada-France-Hawaii Telescope at Mauna Kea. MegaCam images have a field-of-view of ∼1 deg^2 and a 0.187 arcsec/pixel scale. The image set is composed of $u^*g'r'i'z'$ images. The original images were obtained on several nights during October 2005. Details on exposure times and seeing quality can be seen in Table 1. The archive images have been pre-processed (bias subtracted, flat fielded and background subtracted) by the MegaCam pipeline (known as Elixir) and stacked by the MegaCam image stacking pipeline, MegaPipe.

Photometry of the cluster galaxies in the five Megacam bands was performed using SExtractor (Bertin & Arnouts 1996). The full cluster photometry will be presented in a forthcoming publication focusing on the cluster dynamics. Here we present results for the innermost galaxies surrounding the star pile.

2.2. Gemini/GMOS long-slit spectroscopy

Long-slit observations with Gemini South/GMOS (Cerro Pachón, Chile) of the star pile in the center of Abell 545 were carried out during October and November 2007 (program ID GS-2007B-Q-9). Exposure time was 12×2180 s with PA = 209.3 degrees East from North, roughly the star pile's major axis, and 12×2180 s with PA = 151.6 degrees East from North, an intermediate axis of the star pile (see Fig. 1). We used the B600+_G5323 grating and a slit width of 1″ which gives a resolution of ∼6.2 Å *FWHM*.

The spectroscopic reductions were carried out with the aid of the Gemini/IRAF package (version 1.9.1). Bias subtraction, flat fielding and wavelength calibration were performed in the standard way. Typical residuals from the wavelength calibration were ∼0.07 Å. Subsequently, the zero-point of the dispersion solution was checked by measuring the bright sky line at 5577.34 Å and corrected when necessary. These corrections were always less than 0.1 Å. The spectra for each position angle were combined applying a median filter with the IRAF task `lscombine`. These median 2D spectra were sky subtracted using the `background` task inside IRAF.

2.3. FORS2 long-slit spectroscopy

Further long-slit observations were obtained with the Very Large Telescope (VLT) at Cerro Paranal, Chile, using the FORS2/MXU instrument in service mode (program ID 080.B-0529) between November 2007 and March 2008. Long-slit observations were taken with two different position angles: PA = 33.2 degrees East from North, roughly coincident with the apparent photometric major axis of the star pile, and PA = 43.0 degrees East from North, an intermediate axis passing through the eastern apparent nucleus of the star pile and the center of one of the neighbor giant elliptical galaxies that surround the star pile (labeled as C in Fig. 1). The chosen grism was GRIS_1200R+93 with a slit width of 1.31″ which gives a resolution of ∼4 Å *FWHM* in the 5750–7200 Å wavelength range. Both slit positions had an exposure time of 18×1333 s each, i.e. ∼6 h and 40 min.

FORS2 long-slit observations were bias subtracted, flat fielded and wavelength calibrated with the ESO FORS pipeline. Since a large number of exposures were to be combined, no attempt at eliminating cosmic rays on individual images was made. Since the star pile was located on the "master" chip that is expected to give a better performance, only this chip was reduced and further analyzed. Exposures for each PA were median

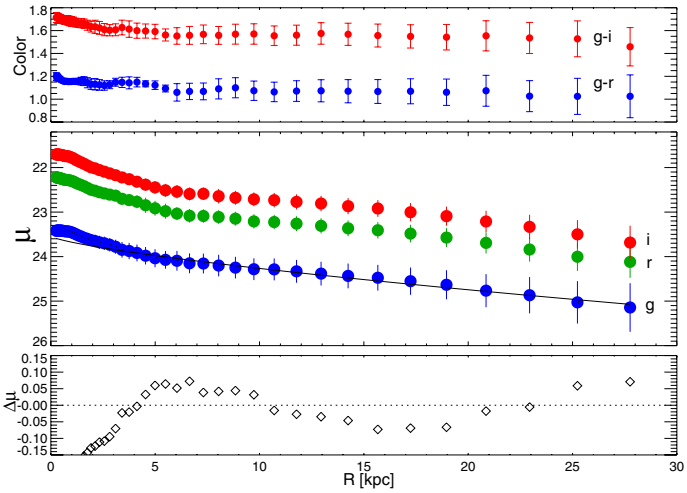

Fig. 2. Azimuthally averaged $g'r'i'$ surface brightness profile of the star pile from the MEGACAM images. The *top panel* shows $g' - r'$ and $g' - i'$ color profiles, while the *lower panel* shows the residuals from the Sérsic fit to the g' photometry.

combined with IRAF/`imcombine`. Sky subtraction done by the ESO FORS pipeline was unsatisfactory so it was performed with the IRAF task `background` by applying a median filter to a clean portion of the sky approximately 50″ NE of the star pile for the PA = 33.2° longslit and 80″ NE for PA = 43°.

The extraction of the FORS2 and GMOS long-slit spectra was done with a custom IDL task. Since the signal from the star pile is weak, it was possible to extract only between one to three radial bins at each side of the "nucleus" inside each slit. Both direct sums and median were used for the spatial binning. Since the surface brightness within the radial bins is not constant, but significantly decreasing due to the large bin size (see Fig. 2), the median was much noisier and unrepresentative of the star pile as a whole, compared with the direct sum, which was therefore chosen for the analysis.

2.4. GMOS and FORS2/MXU multi-object spectroscopy

Additional multi-object spectroscopy of cluster galaxies was taken using GMOS and FORS2. Details of these observations will be presented in a forthcoming publication describing the dynamics of the cluster. Here we present only velocities for the "nuclei" of the star pile as well as its nearest neighbors.

3. Photometric properties of the star pile

S+07 presented *VRI* photometry of the star pile from archival FORS1 images. The photometry was measured using IRAF/`ellipse`, using the galaxy *g2* as the center. The main photometric results from S+07 are: a) the luminosity profile of the star pile is flatter than a typical cD halo; b) there is no evidence for a color gradient inside the star pile; the colors are consistent with an old and metal rich population; and c) the integrated luminosity, including the contribution from *g2*, resembles that of a giant elliptical.

The new spectroscopic data however suggest that the star pile is associated with the galaxy *g3* rather than with *g2* (see Sect. 4.3.1). We re-do the star pile photometry, this time centered on *g3*, using the MEGACAM images, which although obtained under worse seeing conditions, are deeper than the FORS1 images. As with the FORS1 images, the photometry was done with IRAF/`ellipse`, masking neighbor galaxies. For the innermost radii, center, ellipticity and position angle were let free to vary until a radius of 1.5″, where the fit became unstable. Beyond that radius, ellipticity and position angle were kept fixed at $\epsilon = 0.15$ and PA = 33°, and only the center of the ellipses was allowed to vary. $g'r'i'$ photometry can be seen in Fig. 2. The main difference with the FORS1 photometry presented in S+07 is that the transition in the light profile from the *g3* nucleus to the star pile is smoother, indicating perhaps a physical connection, that is not the case of *g2*.

The main findings from S+07 are still valid; the profile presents a mild color gradient in the inner 5 kpc (which can be associated with the nucleus), that can be partially attributed to the slight difference between the image quality in the different photometric bands. Beyond 5 kpc the color profiles are flat within the errors, with values $(g' - r')_0 = 0.94$ and $(g' - i')_0 = 1.33$, where we have corrected for the Galactic absorption (Schlegel et al. 1998). Subtraction of the light model does not reveal any hidden substructure, for example, gravitational arcs.

We fit a Sérsic profile (Sersic 1968; Caon et al. 1993) to the g' photometry, which is less affected by bleeding from the bright star located 20″ South of the star pile (see Fig. 1), outside the inner arcsecond which is affected by seeing. The photometry, excluding the innermost arcsecond (2.74 kpc at the cluster's redshift) is well reproduced by Sérsic parameters $\mu_e = 26.15$, $R_e = 57.3$ kpc and $n = 1.36$. The low value of n indicates that the profile is much flatter than the profile of a typical elliptical galaxy. The Sérsic fit and its residuals can be seen in Fig. 2.

We further model the star pile using a Sérsic profile, in order to address its luminosity and mass profiles. First, the mag/arcsec^2 profile is transformed to a luminosity profile using the distance modulus of 39.39, Galactic absorption $A_g = 0.6$ (Schlegel et al. 1998) and $M_{\odot,g} = 5.12$ (Blanton & Roweis 2007). We also apply the correction for cosmological dimming, $(1+z)^4$. This $L_\odot$ pc^{-2} profile is re-fit with a Sérsic profile of the form,

$$I(R) = I_0 \exp\left[-\left(\frac{R}{a_s}\right)^{\frac{1}{m}}\right], \quad (1)$$

which does not have an exact analytical deprojection, but for which a good analytical approximation exists (Prugniel & Simien 1997),

$$j(r) = j_1 \tilde{j}(r/a_s),$$
$$\tilde{j}(x) \simeq x^{-p}\exp(-x^{1/m}),$$
$$j_1 = \left\{\frac{\Gamma(2m)}{\Gamma[(3-p)m]}\right\}\frac{I_0}{2a_s},$$
$$p \simeq 1 - 0.6097/m + 0.05463/m^2,$$

where the latter equation comes from Lima Neto et al. (1999) and $\Gamma(x)$ is the Gamma function.

Integrating this luminosity density profile, $j(r)$, it is possible to derive an enclosed luminosity. For the Sérsic profile deprojection as given in Eq. (2), the enclosed luminosity has again an analytical expression given by Lima Neto et al. (1999)

$$L_s(r) = L_{tot}\tilde{L}_s(r/a_s), \quad (2)$$
$$\tilde{L}_s(x) = \frac{\gamma[(3-p)m, x^{1/m}]}{\Gamma[(3-p)m]}, \quad (3)$$

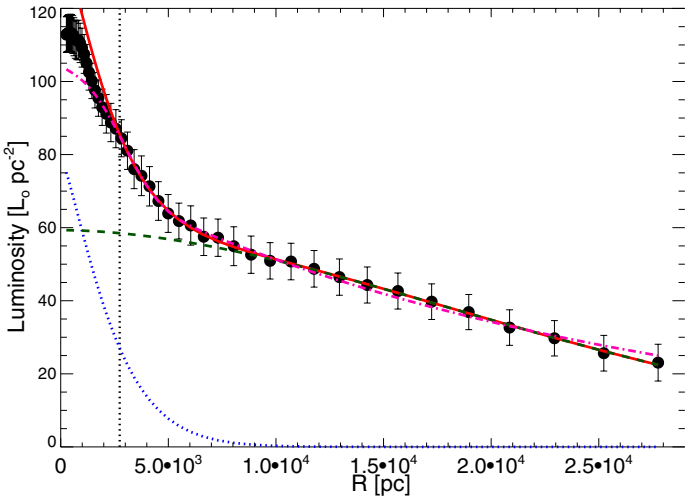

Fig. 3. Star pile g' luminosity profile. The blue dotted line is the Sérsic fit to the nucleus, while the green dashed line is a fit to the extended star pile. The red solid line is the sum of both. The pink dot-dashed line is the Sérsic+exponential model. The radius is the semi-major axis of the fitted ellipses. The vertical dotted line delimits the inner 1″ that was excluded from the fit.

Table 2. Structural parameters of the Sérsic+Sérsic and Sérsic+exponential models of the surface brightness profile of the star pile.

Sérsic + Sérsic	I_0	a_s	m
$\Delta = 0.40$	[$L_\odot$ pc^{-2}]	[kpc]	
inner	79.19	2.588	0.78
outer	58.32	28.178	0.55
Sérsic + exp	I_0	a_s	m
$\Delta = 0.74$	[$L_\odot$ pc^{-2}]	[kpc]	
inner	27.27	3.46	0.35
outer	76.86	24.706	1

where now γ is the incomplete Gamma function and

$$L_{\rm tot} = 2\pi m\Gamma(2m) I_0 a_s^2 \quad (4)$$

is the total luminosity of the profile.

The light profile shows a break in the slope around 5 kpc (see Fig. 3). This could be interpreted as the place where the star pile light starts to dominate over the nucleus if they happen to be different entities. Assuming both *g3* and the star pile form distinct components, we separate them by modeling the luminosity profile as a sum of two Sérsic profiles and also as a Sérsic plus exponential profile, which has been found to give a good fit to cD envelopes (Seigar et al. 2007). Figure 3 shows both models (red and pink lines) as well as the components of the double Sérsic profile. The fit has avoided the inner 1″ which is affected by seeing. We compute the goodness of fit using the rms scatter following Seigar et al. (2007),

$$\Delta = \sqrt{\frac{\sum_i^N \delta_i^2}{N}}, \quad (5)$$

where N is the number of points and the δ_i are the difference in magnitudes between the model and the data. The fit parameters and the goodness of fit of both models can be seen in Table 2. The star pile is better described with the Sérsic profile rather than an exponential. This reinforces the fact that the star pile is something different than a cD envelope.

Using Eq. (2) we calculate the total luminosity of both profiles, $L_{g3} = 2.31 \times 10^9\ L_\odot$ and $L_{\rm sp} = 5.56 \times 10^{10}\ L_\odot$, where the luminosity of the star pile is calculated within the inner 28 kpc, where the photometry has been measured. This luminosity transforms into an absolute magnitude of $M_{g'} = -21.75$ or $M_V = -22.35$ using filter transformations from Blanton & Roweis (2007), that is, almost as luminous as the brightest galaxies in the cluster, and in good agreement with the value given by S+07, $M_V \sim -22.5$, where the measurement included the galaxy *g2*.

Taking the colors $(g' - i')_0 = 1.33$ and $(g' - r')_0 = 0.94$, together with color transformations from Bell et al. (2003), we estimate $M/L_{g'} = 7.7$ for the star pile. This means that the star pile has a stellar mass of $4.3 \times 10^{11}\ M_\odot$ within 30 kpc. Adding *g3*, the baryonic mass slightly increases to $4.5 \times 10^{11}\ M_\odot$.

4. Kinematics of the star pile and its "nuclei"

4.1. Measuring the star pile kinematics

With the spectra presented in S+07 it was possible to confirm the star pile as a cluster feature, but without the sufficient S/N in order to measure a velocity dispersion. The heliocentric radial velocity of the star pile was found to be $47\,100 \pm 60$ km s^{-1}, the uncertainty resulting from the measurements of 16 well identifiable absorption lines. No significant traces of velocity differences were found within the star pile.

With this result in hand, the new spectroscopic observations were planned in order to obtain a velocity dispersion measurement of the star pile. The velocity dispersion of the star pile from the GMOS and FORS2 long-slit observations was determined with the penalized Pixel Fitting code (pPXF, Cappellari & Emsellem 2004). The program selects from a series of templates the best templates that, when convolved with an appropriate line-of-sight velocity distribution, best reproduce the science spectrum. Even though the program allows the extraction of higher order moments of the velocity distribution, this option was suppressed due to the modest S/N of the star pile spectra. As templates we selected the MILES stellar library (Sánchez-Blázquez et al. 2006) that contains 985 stars comprising a wide range of spectral types and metallicities.

After the extraction of the star pile spectra as described in 2.3, and before entering the spectra to pPXF, the spectra were de-redshifted using the IRAF task `dopcor` and using the cluster redshift, $z = 0.15855$ (Salinas et al., in prep.). Afterwards, the spectra were cut in the 4900–5400 Å range in the case of the FORS2 observations, and in the 3900–5000 Å range for the GMOS spectra, both measured in the cluster's rest frame. The blue edge of the FORS spectra was determined by the grism and the red edge was selected to avoid bright sky lines. In the case of the GMOS spectra, the blue edge was taken to include the very noticeable Ca H-K absorption lines. Errors in the measured quantities are obtained by adding noise to 100 Monte Carlo realizations of the extracted spectra and running pPXF over them. The dispersion of the new measurements is quoted as the error in the quantities measured in the original spectrum. Possible systematics in the pPXF measurements introduced during the sky subtraction procedure were explored by constructing sky spectra from both sides of the star pile long-slits. We added/subtracted 5% of the signal to/from these sky spectra before subtracting from the star pile spectra, which then passed pPXF using the procedure outlined before. We find that velocity dispersions changed by at most 15 km s^{-1}, while changes in

Table 3. Star pile velocity dispersion measurements from FORS2 and GMOS longslits.

Instrument/Grism	Radial range [kpc]	PA [degrees]	*S/N*	Δv [km s^{-1}]	σ[km s^{-1}]
FORS2/1200R	5–12	33.2	13	-111 ± 40	299 ± 55
Major axis	12–31	33.2	15	-141 ± 37	255 ± 47
	6–12	213.2	18	-312 ± 40	308 ± 35
	12–29	213.2	14	-308 ± 42	265 ± 32
FORS2/1200R	5.5–15	43.0	13	-27 ± 23	188 ± 31
Interm. axis	2–7	223.0	16	-90 ± 39	129 ± 20
GMOS/600B	5.6–10.4	29.3	9	-91 ± 56	248 ± 26
Major axis	10.4–17.6	29.3	10	-135 ± 57	307 ± 34
	17.6–26.4	29.3	8	-161 ± 57	330 ± 44
	5.6–8.0	209.3	12	-212 ± 41	358 ± 45
	8.0–15.2	209.3	15	-223 ± 31	276 ± 29
	15.2–22.4	209.3	11	-243 ± 134	264 ± 36
GMOS/600B	5.6–9.6	151.6	11	-144 ± 55	120 ± 21
Interm. Axis	9.6–17.6	151.6	10	-133 ± 27	176 ± 15
	4.0–8.8	331.6	14	-252 ± 88	298 ± 21
	8.8–20.8	331.6	12	-343 ± 134	349 ± 25

Notes. Column 1 indicates the instrument/grism combination. Column 2 indicates the radial range in which the spatial binning has been done, with respect to the position of the nucleus the long slit crosses. Column 3 is the position angle of the slit, measured East from North (see Fig. 1 for the exact slit positioning). Column 4 indicates the signal-to-noise ratio of each spectra at the central wavelength of the range used for the pPXF fit. Column 5 is the velocity difference with the system velocity of the cluster. Column 6 indicates the velocity dispersion and its error.

the mean velocities were never larger than 10 km s^{-1} within the uncertainties given by the Monte Carlo procedure.

Galaxy velocities in the Abell 545 field have been measured using IRAF/`fxcor`. For consistency, velocities coming from the different star pile spectra were also measured with this task. To measure a velocity, the high S/N that is required for a velocity dispersion measurement is not necessary, so instead of using the large spatial binning applied for the dispersion calculations, the star pile longslit spectra were spatially rebinned calculating the median of three adjacent pixels. The same wavelength range used for the velocity dispersion measurements was used for these velocity measurements. As templates for `fxcor` we selected 20 old, metal rich single stellar population models from Vazdekis et al. (2010). The velocities and errors given in Fig. 5 and in Table 4 were taken as the mean results from the five templates which gave the highest cross-correlation peak. These have ages between 7–14 Gyr and metallicities $[M/H] = 0.0–0.2$. The zero-point of the velocity calibration between the galaxies and the longslits was determined by the comparison of the measured velocities of galaxies C and *g3* (see Fig. 6) which they had in common. The velocities from both spectroscopic methods agree within the errors.

4.2. The star pile kinematics: results

The results of the pPXF fitting for the different long slits and the velocity determination with `fxcor` can be seen in Table 3. A visual representation of this table, together with velocities and velocity dispersions, when available, for neighboring galaxies, is given in Fig. 6. Velocity measurements with the low spatial binning can be seen in Fig. 5.

4.2.1. The star pile velocity map

The first, and most surprising result is the fact that the star pile, or at least a substantial part of it, does not seem to be at rest at the bottom of the potential well as expected. All the long slit mean velocity measurements point to a velocity difference of ∼100−500 km s^{-1} less than the cluster systemic velocity. The major axis velocity measured from the GMOS and FORS2 longslits agree within the errors (Fig. 5, left panel). We note that a significant difference exists between the sections of the star pile located North (positive radii in left panel of Fig. 5) and South (negative radii) of the galaxy *g2* that the major axis longslit crosses. While the South part has a mean velocity difference with the cluster velocity of −300 km s^{-1}, the difference of the North section is −160 km s^{-1}. Since the uncertainty of the cluster mean velocity is ±84 km s^{-1} (Salinas et al., in prep.), it is possible to consider some parts of the star pile as at rest compared the cluster. This specially applies to the zones nearest to *g3* (see Fig. 5, right panel).

The GMOS intermediate axis (blue points in the right panel of Fig. 5) gives the most extreme velocity differences. In the North-West part of the star pile, the mean velocity reaches a ∼450 km s^{-1} difference with the cluster velocity. A couple of measurements reach even larger velocities. The one at $R \sim 0$ kpc, with $v \sim -600$ km s^{-1}, is possibly contaminated by the spectrum of the high velocity galaxy *g2*. The measurements at $R \sim 20$ kpc are more difficult to explain. Even though the nearby galaxy (labeled "D" in Figs. 1 and 6) has a similar rest frame velocity, $v = -437 \pm 42$ km s^{-1}, it seems too distant to be contaminating this section of the star pile. It is also interesting to mention that this longslit crosses a very faint source, which we have labeled *g6*, that is only visible in the FORS1 V image (which has the best seeing in all our imaging dataset). It is not possible to say if this is an independent source (nucleus or background galaxy) or some substructure within the star pile. However, the source is unlikely to influence the velocity dispersion in the NW part of the star pile due to its low surface brightness.

4.2.2. The star pile velocity dispersion

The tumultuous picture given by the velocities is reinforced by the velocity dispersion measurements. GMOS and FORS2 velocity dispersion measurements can be seen in Table 3 and Fig. 6. The GMOS major axis shows an increase in the velocity dispersion in the NE direction, but a decrease in the SW direction. The FORS2 major axis has a good agreement in the SW velocity dispersion and a worse agreement in the NE part, preferring

Table 4. Photometry of the star pile "nuclei" and neighbor member galaxies depicted in Fig. 6.

ID	RA	Dec	D [kpc]	u^*	g'	r'	i'	z'	cz [km s^{-1}]	$v_{\rm pec}$ [km s^{-1}]
g1	05:32:24.93	–11:32:38.20	19.5	23.61	21.67	20.53	19.99	19.52	46 608 ± 48	–792 ± 97
g2	05:32:25.19	–11:32:39.23	8.2	24.53	22.64	21.59	21.09	20.66	45 772 ± 28	–1514 ± 85
g3	05:32:25.39	–11:32:40.07	0.0	24.97	23.07	21.89	21.39	20.89	47 511 ± 35	–13 ± 91
A	05:32:26.46	–11:32:37.92	43.5	21.22	19.08	18.11	17.61	17.59	46 096 ± 24	–1234 ± 87
B	05:32:26:44	–11:32:42.39	42.4	23.47	21.60	20.57	20.03	19.92	45 018 ± 28	–2164 ± 88
C	05:32:25.79	–11:32:33.72	23.7	20.39	18.57	17.53	16.99	16.68	47 338 ± 62	–162 ± 104
D	05:32:24.63	–11:32:29.96	41.5	21.31	19.61	18.58	18.06	17.68	47 019 ± 42	–437 ± 94
E	05:32:24.44	–11:32:43.51	39.6	21.04	19.24	18.30	17.68	17.48	48 208 ± 50	588 ± 98
F	05:32:24:18	–11:32:32.16	53.6	21.24	19.46	18.40	17.84	17.47	48 525 ± 42	862 ± 94
G	05:32:23.81	–11:32:45.46	65.9	20.53	18.44	17.35	16.79	16.50	46 318 ± 35	–1042 ± 91

Notes. Column 1 is the galaxy ID. Columns 2 and 3 indicate the celestial coordinates. Column 4 is the projected distance to the cluster center in kpcs, which is taken at the position of galaxy *g3*. Columns 5–7 are the $u^*g'r'i'z'$ AB photometry. Column 8 is the recessional heliocentric velocity and Col. 9 is the peculiar rest frame velocity.

lower velocity dispersions. The intermediate axis long slits show that the vicinity of the galaxy *g3* has velocity dispersions below 200 km s^{-1}, and that the NW part of the star pile has an increasing velocity dispersion profile, similar to the NE part.

The kinematic information from the long slits shows that a significant part of the star pile, ∼10 kpc in radius from *g3*, seems to be kinematically connected to this galaxy, with consistent velocities and velocity dispersions. The rest of the star pile has very different velocities from the cluster mean velocity (that is the same as *g3*) and larger velocity dispersions. This makes a dynamical connection for these parts of the star pile to the galaxy *g3* or any surrounding galaxy doubtful, although it cannot be discarded that they were once part of *g3*, but now have gained velocity due to some complex dynamic interactions.

4.3. The star pile "nuclei"

As already mentioned in Sect. 1 and as can be seen in Fig. 1, the star pile appears to have at least three nuclei. Multiple nuclei are not an uncommon phenomenon in brightest cluster galaxies (BCGS, Hoessel & Schneider 1985; Laine et al. 2003), although their physical connection with the central galaxy is doubtful (Tonry 1985; Blakeslee & Tonry 1992). In Fig. 1 these are labeled as *g1*–*g6*, for consistency with the names adopted in S+07. In this section we describe the observations of the three brightest, *g1*–*g3*. One of the aims of our MOS campaigns was to establish if these sources that seem embedded in the star pile were, in the first place, real cluster members, and secondly, if from their velocity it could be argued that they are actually nuclei of the central feature, or galaxies in the process of merging with the star pile.

S+07 presented photometry of the nuclei using the FORS1 images. The most important results are: a) the apparent magnitudes and colors of the nuclei are consistent with low-luminosity ellipticals, and b) while sources *g2* and *g3* have normal sizes, source *g1* has a compact nature, with an effective radius of about 400 pc. Here we expand the discussion on the star pile nuclei using the new kinematic information and in the context of the MEGACAM photometry.

4.3.1. Nuclei kinematics

The radial velocity of the source *g2* was already determined in S+07 and found to be ∼1300 km s^{-1} less than the star pile velocity. This velocity has been refined with the new spectroscopy and now has the value of 45 772 ± 28 km s^{-1}, in very good agreement with the previous measurement. The very large velocity offset rules out the idea of this source as a nucleus of the star pile, but is not enough to classify this galaxy as a non-member of the cluster. Its projected position, so close to the galaxy cluster center, and its large line-of-sight velocity, provide evidence for a very radial orbit close to the line of sight that has reached or is about to reach the bottom of the potential well. Sources *g1* and *g3* have been also confirmed to be cluster members with the new measurements. Their radial velocities are 46 608 ± 48 km s^{-1} and 47 511 ± 35 km s^{-1}, respectively. Their peculiar velocities can be seen in Table 4. The velocity of *g1* also argues against it being a nucleus of the star pile, but the velocity of *g3* places it exactly at the center of the velocity distribution, making it the most probable "central galaxy" of the cluster.

The large exposure times for *g2* and *g3*, which were inside the slits for measuring the kinematics of the star pile as seen in Fig. 1, prompted us to obtain a velocity dispersion for these galaxies. Unfortunately, even though the S/N seemed sufficient, the resolution of the 1200R grism was not, and even though pPXF gives a good fit, it failed to give a meaningful value for the velocity dispersion in the case of *g2*. Looking at the spectrum of *g2*, the Mg I doublet (5167 and 5172 Å) looks clearly resolved, so we estimate the velocity dispersion for this galaxy to be $\lesssim$70 km s^{-1}, again consistent with a low luminosity elliptical galaxy. In the case of *g3*, using pPXF we calculate a velocity dispersion of 110 ± 11 km s^{-1}. The pPXF fit to this galaxy can be seen in Fig. 4.

The fact that the dimmer galaxy *g3* has a larger velocity dispersion than its brighter neighbor *g2* clashes with the expectations from scaling relations (Faber & Jackson 1976). Keeping in mind the difficulties in measuring total magnitudes for these sources we can compare the dispersion values of *g2* and *g3* with the measured velocity dispersions for nearby dEs. While *g2* has a normal velocity dispersion for its brightness, *g3*'s velocity dispersion is too high when compared with the values obtained for dEs in nearby clusters (e.g. Spolaor et al. 2010). Three explanations are possible for this behaviour. First, that the galaxy was brighter in the past, but has been tidally stripped, remembering its original central velocity dispersion. Second, would be the expected increase in the dispersion induced by harrasment (Moore et al. 1998), although this process also predicts an increase in the central luminosity density which would mean the galaxy had an even lower original surface brightness. The final possibility is that the particular position of the galaxy near to the cluster center makes it dark matter dominated even to its inner regions. This last option will be explored in a forthcoming paper.

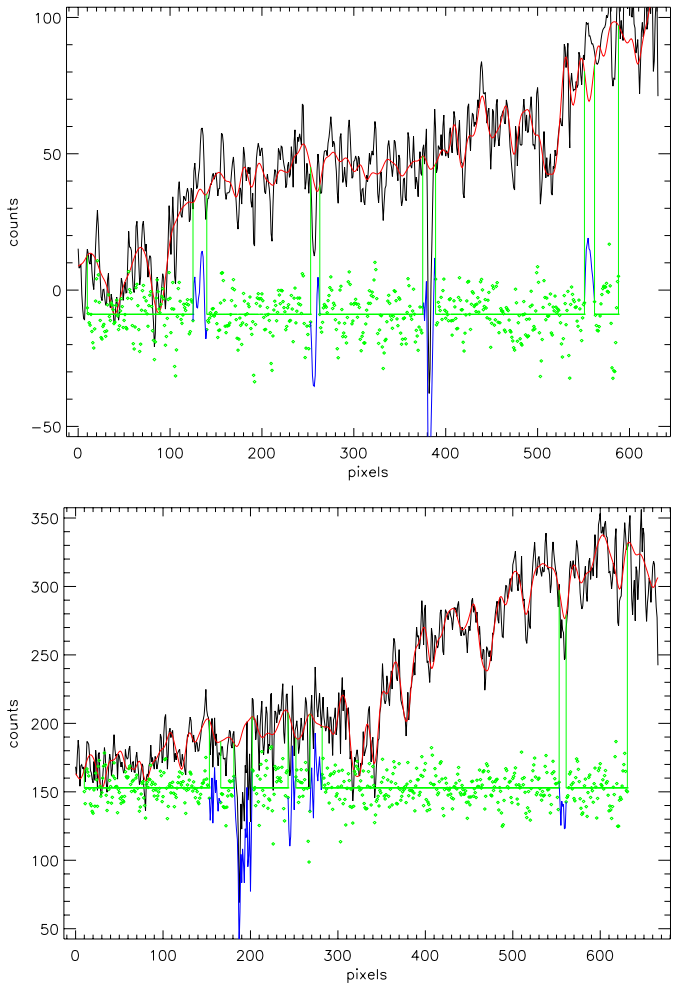

Fig. 4. Examples of spectra and pPXF fits. *Top panel*: the star pile spectrum in the 9–21 kpc range coming from GMOS intermediate axis longslit. *Bottom panel*: *g3* nucleus spectrum from the FORS2 data. In both panels the original spectrum is drawn in black, while the fit is in red. Green points indicate the fit residuals, and blue portions indicate ranges that were excluded from the fit due to their large residuals from ill-subtracted sky lines or other artifacts. The wavelength range is 3900–4400 Å and 4900–5400 Å for the top and bottom panels, respectively, in the rest frame.

Aguilar & White (1986) analyzed the effect on the density profiles of galaxies that have undergone a tidal encounter. One of their main conclusions is that strong encounters would increase the surface brightness and reduce the effective radius in the affected galaxy. The exact opposite effects are expected for weak encounters. The difference between strong and weak encounters lies on a combination of the mass ratio of the participant galaxies, their relative velocities and impact parameter. In the center of Abell 545 we can imagine a similar situation where the nuclei have an encounter with the cluster's dark matter halo. For the nuclei, their mass ratio compared to the dark halo and the impact parameter can be considered as equal. The main diffrence would be their velocities; while the high-speed galaxy *g2* has been unaffected in its structure, the mid-speed galaxy *g1* has presumably suffer a strong encounter, loosing its outer regions and mutating into a compact source. Finally, the low-speed galaxy *g3* has undergone a weak collision, lowering its surface brightness and seeming to be on the verge of complete tidal disruption.

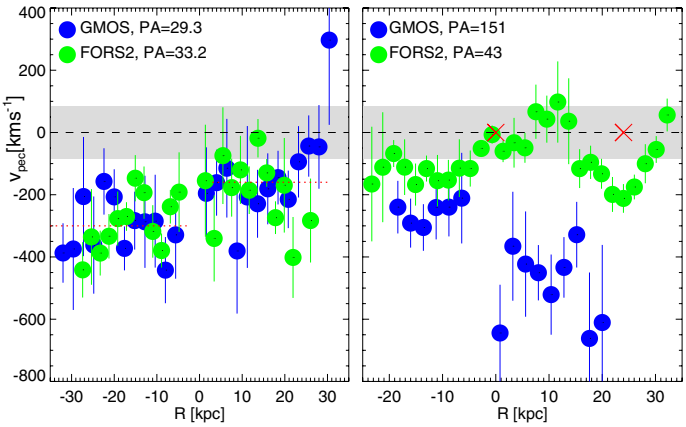

Fig. 5. Velocity measurements from FORS2 (blue symbols) and GMOS (green symbols) with respect to the cluster velocity. The shaded grey area indicates the 1-σ confidence level for the cluster mean redshift. The zero point of the radii is defined by the position of the nuclei over which the long slit is placed. *Left panel*: major axis velocity profile, the red dotted lines indicate the mean velocities North and South of the central galaxy. *Right panel*: the two intermediate axis velocity profiles. The red crosses in the center mark the positions of the galaxies *g3* and "C" that the FORS2 longslits crosses.

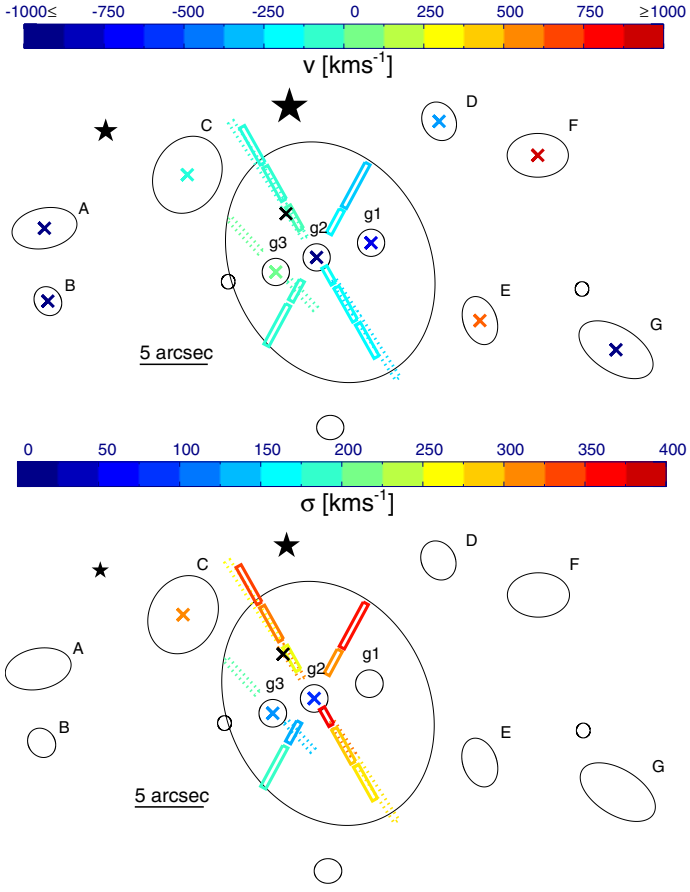

Fig. 6. 2-D kinematics representation at the center of Abell 545. Ellipses indicate the positions for member galaxies and the star pile. Crosses indicate the measurements for member galaxies from the MOS campaigns, while the rectangles indicate the measurements from the GMOS (solid line) and FORS2 (dotted line) long-slits. Star symbols indicate the position of two spectroscopically confirmed Galactic stars. *Top panel*: peculiar velocities at the center of Abell 545. *Bottom panel*: velocity dispersion measurements. In both panels, the black X symbol indicates the central position of the X-ray emission given by David et al. (1999). Figure scale is the same as in Fig. 1. North is up, East to the left.

5. The absence of a central galaxy and the origin of the star pile

Many lines of observational evidence point to cD galaxies as a family different from giant elliptical galaxies (e.g. Dressler 1978; Kormendy & Djorgovski 1989; von der Linden et al. 2007). This has prompted the development of many theories and models for their formation (e.g. Merritt 1984; Fabian 1994; Dubinski 1998; De Lucia & Blaizot 2007). However, theoretical studies on the *lack* of cD formation in some cluster centers is scarce.

How does the star pile compares to the properties of cD envelopes? First, although it has a large size, with ~60 kpc on its major axis (Struble 1988, S+07), it is still small compared to cD sizes which can extend to hundreds of kpc (Schombert 1986). Second, as we have shown in Sect. 3, the light profile is much flatter than that of a cD envelope, and the same time, with a total luminosity of $L \sim 5 \times 10^{10}\ L_{\odot}$, it falls short compared to the values for cD envelopes which have luminosities between 10^{11}–$10^{12}\ L_{\odot}$ (Schombert 1986). On the other hand, the fact that the peculiar velocity of the star pile is non-zero does not necessarily rule it out as a cD envelope, since cD galaxies can have significant velocity offsets with respect to their cluster velocity (Zabludoff et al. 1990; Oegerle & Hill 2001; Pimbblet et al. 2006).

One possibility, proposed by S+07, is that the large velocity dispersion in the center of massive clusters prevents the formation of a cD. Within the inner 100 kpc the velocity dispersion of the cluster galaxies reaches ~900 km s^{-1} (Salinas et al., in prep. and see also Table 4). Strong tidal forces might disrupt any attempt of galaxy formation. Tidal forces and stripping are definitely at play at the center of the cluster, and this is reflected in the compact nature of the galaxy *g1* and the extended, and seemingly dissolving, galaxy *g3*. The luminosity of the star pile is larger than the predictions for the growth of a central galaxy through "cannibalism" (1–2 $L^{\star}$, Merritt 1985; Lauer 1988). If stripping is the main origin of the star pile it is not produced by a central galaxy which is absent, indicating that stripping is mainly driven by the underlying dark matter halo.

Intracluster light (hereafter ICL) is the name given to all the stellar populations that inhabit a cluster, but that are not gravitationally bound to any galaxy in particular but to the cluster potential (Arnaboldi & Gerhard 2010, and references therein). In practice, to determine if stars (or planetary nebulae, or globular clusters) are bound or not to a galaxy is difficult, requiring kinematic information rarely available. Instead, ICL is usually handled with a working definition, for example, Zibetti et al. (2005) uses $\mu_r > 25$ as a photometric threshold. Simulations predict that most of the ICL component is produced during the series of mergers which become a BCG, disfavouring a tidal origin (Abadi et al. 2006; Murante et al. 2007).

As seen in previous sections, parts of the star pile can be considered as an extension of the galaxy named *g3*, while other parts, especially the North-West, have a significant velocity difference with the systemic velocity and the velocities of neighbor galaxies. So perhaps we are seeing the first diffuse ICL component defined dynamically, besides planetary nebulae and globular clusters found in galaxy clusters at lower redshifts (e.g. Arnaboldi et al. 2004; Bergond et al. 2007). But if we go back to the photometric definition of Zibetti et al. (2005), we find that the entire star pile has a higher surface brightness than the definition with $\mu_r < 24.5$. It is also higher than the values predicted by simulations (Willman et al. 2004). Perhaps ICL as bright as this is formed usually in massive clusters but is captured by a central galaxy which masks its presence.

One further note refers to the regular appearance that the star pile shows, which is at odds with irregular structures such as tails and arcs that have been identified as ICL in nearby clusters (e.g. Trentham & Mobasher 1998; Gregg & West 1998; Mihos et al. 2005). These cold structures are expected to decay rapidly (1 Gyr) on the central parts of galaxy clusters (Rudick et al. 2009), so this can be an indication that the star pile is in a more evolved dynamical stage, but, on the other hand, the existence of significant velocity differences within the star pile could be considered as evidence for unmixed material as in the halos of nearby central galaxies (McNeil et al. 2010; Ventimiglia et al. 2011). Perhaps its seemingly smooth appearance is the effect of several overlapping irregular features, but this speculation must await support from higher resolution imaging (e.g. with the HST).

The center of Abell 3827 has some resemblance to the center of Abell 545 (Carrasco et al. 2010). Abell 3827 contains a massive cD galaxy in the apparent process of devouring four smaller galaxies. The peculiar velocities of these galaxies respect to the systemic velocity are ~100 km s^{-1} for two of them, ~300 km s^{-1} for another and ~1000 km s^{-1} for the last one. So, as in Abell 545, there are galaxies that presumably have been slowed down by dynamical friction while the other is making a first passage through the cluster center. Another related system is the galaxy cluster CL 0958+4702, where three galaxies are probably merging with the BCG producing a large plume of stars (Rines et al. 2007). This diffuse halo has a similar surface brightness to the star pile and a very similar luminosity $L_r \sim 5 \times 10^{10}\ L_{\odot}$. A key difference is the low velocity dispersion of the inner galaxy population in CL 0958+4702 with $\sigma \sim 250$ km s^{-1}. Galaxy interactions are favored in low velocity dispersion systems (e.g. Osmond & Ponman 2004). Another key difference is that in CL 0958+4702, the origin of the plume has a natural explanation as by-product of a major merger which would eventually become a BCG. This is not the case in Abell 545, where there is no evidence of an on-going major merger, nor the possible formation of a BCG.

6. Summary and conclusions

The "star pile" is an extended feature of approximately elliptical appearance of low surface brightness with three embedded "nuclei" in the center of the massive galaxy cluster Abell 545, in which a cD galaxy is otherwise absent. We present new kinematical details regarding the star pile and its nuclei. Deep long-slit observations reveal a velocity field which clearly disfavor the projected central object named *g2* as the spatially central nucleus of the star pile due to its large velocity offset of −1500 km s^{-1}. Somewhat suprisingly, the Eastern nucleus (*g3*) is kinematically connected to at least parts of the star pile. The velocity field of the star pile itself in the regions probed by the long-slits shows moderate offsets around −100 km s^{-1} in the Eastern part and reaches as high as −450 km s^{-1} in the North-Western part.

The velocity dispersion neither does exhibit a simple pattern. In the proximity of *g3* it shows moderate values of 100–150 km s^{-1}, similar to *g3*, but rises along the major axis to the NE to values of around 300 km s^{-1}, but declines or stays constant towards the SW at values of around 200–300 km s^{-1}. The highest values of around 350 km s^{-1} are found towards the NW.

The star pile origin is most probably connected to the tidal stripping of at least one galaxy that now appears as its nucleus. It is not possible to say if the stripping proccess was produced by

the interaction with the other embedded sources or by a tidal interaction with the cluster potential, which stand as the two most likely origin explanations. The star pile could serve as a probe for the inner cluster dark matter profile, only if the kinematics of its nucleus *g3* and its near surroundings, which seem at rest with respect to the cluster potential, are considered.

Acknowledgements. We thank an anonymous referee for a quick and helpful report. R.S. acknowledges support from a CONICYT doctoral scholarship and the ESO studentship programme. T.R. acknowledges financial support from the Chilean Center for Astrophysics, FONDAP Nr. 15010003, from FONDECYT project Nr. 1100620, and from the BASAL Centro de Astrofisica y Tecnologias Afines (CATA) PFB-06/2007. A.J.R. was supported by National Science Foundation grants AST-0808099 and AST-0909237.

References

Abadi, M. G., Navarro, J. F., & Steinmetz, M. 2006, MNRAS, 365, 747
Aguilar, L. A., & White, S. D. M. 1986, ApJ, 307, 97
Arnaboldi, M., & Gerhard, O. 2010, Highlights of Astronomy, 15, 97
Arnaboldi, M., Gerhard, O., Aguerri, J. A. L., et al. 2004, ApJ, 614, L33
Bell, E. F., McIntosh, D. H., Katz, N., & Weinberg, M. D. 2003, ApJS, 149, 289
Bergond, G., Athanassoula, E., Leon, S., et al. 2007, A&A, 464, L21
Bertin, E., & Arnouts, S. 1996, A&AS, 117, 393
Blakeslee, J. P., & Tonry, J. L. 1992, AJ, 103, 1457
Blanton, M. R., & Roweis, S. 2007, AJ, 133, 734
Caon, N., Capaccioli, M., & D'Onofrio, M. 1993, MNRAS, 265, 1013
Cappellari, M., & Emsellem, E. 2004, PASP, 116, 138
Carrasco, E. R., Gomez, P. L., Verdugo, T., et al. 2010, ApJ, 715, L160
Cowie, L. L., & Binney, J. 1977, ApJ, 215, 723
David, L. P., Forman, W., & Jones, C. 1999, ApJ, 519, 533
De Lucia, G., & Blaizot, J. 2007, MNRAS, 375, 2
Del Popolo, A., & Kroupa, P. 2009, A&A, 502, 733
Dressler, A. 1978, ApJ, 223, 765
Dressler, A. 1980, ApJ, 236, 351
Dubinski, J. 1998, ApJ, 502, 141
El-Zant, A. A., Hoffman, Y., Primack, J., Combes, F., & Shlosman, I. 2004, ApJ, 607, L75
Faber, S. M., & Jackson, R. E. 1976, ApJ, 204, 668
Fabian, A. C. 1994, ARA&A, 32, 277
Gnedin, O. Y., Kravtsov, A. V., Klypin, A. A., & Nagai, D. 2004, ApJ, 616, 16
Gregg, M. D., & West, M. J. 1998, Nature, 396, 549
Hoessel, J. G., & Schneider, D. P. 1985, AJ, 90, 1648
Kelson, D. D., Zabludoff, A. I., Williams, K. A., et al. 2002, ApJ, 576, 720
Kormendy, J., & Djorgovski, S. 1989, ARA&A, 27, 235
Laine, S., van der Marel, R. P., Lauer, T. R., et al. 2003, AJ, 125, 478
Lauer, T. R. 1988, ApJ, 325, 49
Lima Neto, G. B., Gerbal, D., & Márquez, I. 1999, MNRAS, 309, 481
Macciò, A. V., Dutton, A. A., & van den Bosch, F. C. 2008, MNRAS, 391, 1940
McNeil, E. K., Arnaboldi, M., Freeman, K. C., et al. 2010, A&A, 518, A44
Merritt, D. 1984, ApJ, 276, 26
Merritt, D. 1985, ApJ, 289, 18
Mihos, J. C., Harding, P., Feldmeier, J., & Morrison, H. 2005, ApJ, 631, L41
Moore, B., Lake, G., & Katz, N. 1998, ApJ, 495, 139
Murante, G., Giovalli, M., Gerhard, O., et al. 2007, MNRAS, 377, 2
Navarro, J. F., Frenk, C. S., & White, S. D. M. 1996, ApJ, 462, 563
Oegerle, W. R., & Hill, J. M. 2001, AJ, 122, 2858
Osmond, J. P. F., & Ponman, T. J. 2004, MNRAS, 350, 1511
Ostriker, J. P., & Tremaine, S. D. 1975, ApJ, 202, L113
Pimbblet, K. A., Roseboom, I. G., & Doyle, M. T. 2006, MNRAS, 368, 651
Prugniel, P., & Simien, F. 1997, A&A, 321, 111
Richstone, D. O. 1976, ApJ, 204, 642
Rines, K., Finn, R., & Vikhlinin, A. 2007, ApJ, 665, L9
Rudick, C. S., Mihos, J. C., Frey, L. H., & McBride, C. K. 2009, ApJ, 699, 1518
Salinas, R., Richtler, T., Romanowsky, A. J., West, M. J., & Schuberth, Y. 2007, A&A, 475, 507
Sánchez-Blázquez, P., Peletier, R. F., Jiménez-Vicente, J., et al. 2006, MNRAS, 371, 703
Sand, D. J., Treu, T., Smith, G. P., & Ellis, R. S. 2004, ApJ, 604, 88
Sand, D. J., Treu, T., Ellis, R. S., Smith, G. P., & Kneib, J.-P. 2008, ApJ, 674, 711
Schlegel, D. J., Finkbeiner, D. P., & Davis, M. 1998, ApJ, 500, 525
Schombert, J. M. 1986, ApJS, 60, 603
Seigar, M. S., Graham, A. W., & Jerjen, H. 2007, MNRAS, 378, 1575
Sersic, J. L. 1968, Atlas de galaxias australes, ed. J. L. Sersic
Spolaor, M., Hau, G. K. T., Forbes, D. A., & Couch, W. J. 2010, MNRAS, 408, 254
Struble, M. F. 1988, ApJ, 330, L25
Tonry, J. L. 1985, AJ, 90, 2431
Trentham, N., & Mobasher, B. 1998, MNRAS, 293, 53
Vazdekis, A., Sánchez-Blázquez, P., Falcón-Barroso, J., et al. 2010, MNRAS, 404, 1639
Ventimiglia, G., Arnaboldi, M., & Gerhard, O. 2011, A&A, 528, A24
von der Linden, A., Best, P. N., Kauffmann, G., & White, S. D. M. 2007, MNRAS, 379, 867
Whitmore, B. C., Gilmore, D. M., & Jones, C. 1993, ApJ, 407, 489
Willman, B., Governato, F., Wadsley, J., & Quinn, T. 2004, MNRAS, 355, 159
Zabludoff, A. I., Huchra, J. P., & Geller, M. J. 1990, ApJS, 74, 1
Zibetti, S., White, S. D. M., Schneider, D. P., & Brinkmann, J. 2005, MNRAS, 358, 949